Differential Tractography as a Track-Based Biomarker for Neurodegeneration

Authors: Fang-Cheng Yeh[1,2,*], Islam M. Zaydan[3], Valerie R. Suski[3], David Lacomis[3,4], R. Mark Richardson[1], Joseph C. Maroon[1], and Jessica Barrios-Martinez[1]

Affiliations:

[1]Department of Neurological Surgery, University of Pittsburgh School of Medicine, Pittsburgh, Pennsylvania, United States

[2]Department of Bioengineering, University of Pittsburgh, Pittsburgh, Pennsylvania, United States

[3]Department of Neurology, and the [4]Live Like Lou Center for ALS Research, University of Pittsburgh School of Medicine, Pittsburgh, PA, United States

*Correspondence to:

Fang-Cheng Yeh, M.D. Ph.D.

Department of Neurological Surgery,

Department of Bioengineering,

University of Pittsburgh, Pittsburgh, Pennsylvania

Email: frank.yeh@pitt.edu

One Sentence Summary:

Differential tractography utilizes repeat diffusion MRI scans of the same subject to identify tracks with neurodegeneration.

Abstract

Diffusion MRI tractography has been used to map the axonal structure of human brain, but its ability to detect neurodegeneration is yet to be explored. Here we report differential tractography, a new type of tractography that utilizes a novel tracking strategy to map the exact segment of fiber pathways with neurodegeneration. It utilizes voxel-wise differences from repeat scans and aggregates them as track-based biomarkers for neurodegeneration. We examined differential tractography on multiple sclerosis, Huntington disease, amyotrophic lateral sclerosis, and epileptic patients. The results showed that the affected pathways shown by differential tractography matched well with the unique clinical symptoms of the patients, and the false discovery rate of the findings could be estimated using a sham setting to provide a reliability measurement. This novel approach enables a quantitative and objective method to monitor neurodegeneration in individuals, allowing for diagnostic and prognostic evaluation of brain diseases.

Keywords: diffusion MRI, differential tractography, fiber tracking, imaging biomarker, neurodegeneration, axonal injury.

Introduction

Magnetic resonance imaging (MRI) is a commonly used neuroimaging technique for revealing neurodegeneration in patients with neurological disorders. Studies have used structural MRI to reveal gray matter atrophy in patients with multiple sclerosis[1,2] and atrophy in the caudate in patients with Huntington disease[3,4]. In addition to structural MRI, diffusion MRI has also been explored as an imaging biomarker for early-stage neurodegeneration before atrophy happens. Animal studies have used diffusion tensor imaging (DTI)[5] to detect acute demyelination or axonal loss [6,7]. The decrease of anisotropic diffusion (a.k.a. anisotropy), has been shown to be correlated with axonal loss or neurodegeneration [8-11]. However, anisotropy remains a voxel-based measurement, which is prone to local variations such as partial volume effect [12,13] or signal noise, thereby limiting its clinical applications [14]. Greater specificity and sensitivity could be achieved by aggregating voxel-wise anisotropy changes along fiber pathways and grouping them into a "track".

To this end, we propose a novel method called "differential tractography" to provide a track-based biomarker of neurodegeneration. This method compares repeat scans of the same individuals to capture neurodegeneration reflected by a decrease of anisotropic diffusion, or "anisotropy" (Fig 1a-1c). To achieve a higher specificity, we imbued the deterministic fiber tracking algorithm[15] with a novel "*tracking-the-difference"* paradigm. This was realized by adding an additional criterion that tracks along trajectories on which a decrease of anisotropy was found between repeat scans (Fig. 1d-1e). Integrating this "tracking-the-difference" paradigm into the fiber tracking process resulted in a new tractography approach that can track the exact portion of pathways exhibiting substantial differences in anisotropy. The additional criterion will ignore unaffected regions and enhance meaningful findings related to

neurodegeneration. In comparison, the conventional fiber tracking [16] is based on a "*tracking-the-existence*" paradigm. It only considers anisotropy from one MRI scan and thus will include all existing pathways regardless of whether they have a decrease in the anisotropy.

To further maximize the detection power, we used a diffusion MRI acquisition that sampled 22 diffusion sensitizations at 257 directions, a substantial improvement over one sensitization at 30~60 directions used in the conventional settings, or 3 diffusion sensitizations at 180 directions used in the current mainstream studies [17]. The higher number of diffusion sensitizations greatly increased the chance of diffusion MRI to detect early-stage neurodegeneration that involves only a subtle change in the restricted diffusion [12]. These multiple sensitizations allowed us to derive an anisotropy measurement that has a different biophysical meaning from the fractional anisotropy (FA) of DTI (see Discussion) and has been shown to be more robust against partial volume effect[12,15]. We also introduce a novel sham setting that can estimate the false discovery rate (FDR) of differential tractography to provide a reliability measurement against local random error.

To evaluate the performance, we applied differential tractography to patients with four different clinical scenarios at different stages of neurodegeneration (demographic information listed in Table 1). The first scenario was multiple sclerosis (MS) with the first episode of optic neuritis. The baseline scans were acquired during the onset, and the follow-up diffusion MRI scans were acquired 6 months after. This scenario tested differential tractography at the early stage of neurodegeneration to explore its sensitivity, and any meaningful findings should be located near the visual pathways. The second scenario was the manifested Huntington disease (HD) with worsening clinical motor scores during the interval of their

repeat MRI scans. We examined whether differential tractography could detect progressing neurodegeneration at striatal pathways that are commonly affected by the disease. The third scenario studied the neurodegeneration in an ALS patient with a deteriorating functional motor score. We examined whether differential tractography could be correlated with the patient's clinical presentation. Last, we applied differential tractography to an epileptic patient treated by anterior temporal lobectomy. The baseline scan was acquired before the surgery, and the follow-up scan was acquired one year after the surgery. This examined whether differential tractography could correctly locate pathways with established neurodegeneration after surgery, and meaningful findings should be in pathways previously connected to the area of resection. We also applied differential tractography to a normal subject to demonstrate how differential tractography may capture false results.

Results

Neurodegeneration reflected by a decrease of anisotropy

Figure 2a shows the intermediate results of differential tractography applied to an MS patient with optic neuritis (patient #1, demographics summarized in Table 1). The baseline scan was acquired during the onset, whereas the follow-up scan was acquired 6 months after. Differential tractography first compares, voxel-by-voxel, the anisotropy of repeat MRI scans in a common subject space (Fig. 1a-1c) to identify local differences as shown by the red sticks in Fig. 2a. The red sticks represent local fiber orientations with a decrease of anisotropy greater than 30% (This 30% threshold is termed "anisotropy threshold" hereafter). Most of the differences are distributed near the primary visual pathways, whereas some spurious differences are randomly distributed throughout the entire whiter matter regions, most likely due to local signal variations or registration error.

To eliminate these local spurious differences, the “tracking-the-difference” algorithm is applied to the track and link all local differences together into continuous trajectories, and short fragments are discarded using a length threshold of 40 mm (Fig. 2b). The rationale behind this length threshold is that the local random error does not propagate along fiber pathways, whereas true findings due to neurodegeneration will form a decrease of anisotropy along a fiber bundle. A length threshold will effectively differentiate between them and retain true findings.

The left inset figure in Fig. 2b shows affected tracks in directional colors (red: left-right green: anterior-posterior blue: superior-inferior), whereas the tracks in the right inset figure are color-coded by the percentage decrease of anisotropy suggesting the severity of neurodegeneration (yellow: 0% decrease red: 70% decrease). In overall, the differential tractography in Fig. 2b reveals a heterogenous decrease of anisotropy between 20% to 50%. All findings are in the bilateral primary visual pathways or their collateral connections. The location of the finding matches well with the patient’s medical history of visual field loss in both left and right quadrants. The topology of affected pathways seems to present a ripple effect: not only the primary visual pathway is affected, but also certain collateral connections to the visual cortex has shown a decrease in the anisotropy. Although this patient was fully recovered from the symptoms during the follow-up scan (brief medical history in the Supplementary materials), differential tractography still captures subclinical change near the bilateral optic radiation.

Conventional tractography versus differential tractography

Figure 3 compares conventional tractography (Fig. 3a) with differential tractography (Fig. 3b) on another MS patient with optic neuritis (patient #2 demographics summarized in Table 1). The conventional tractography was generated using the baseline scan, whereas the differential tractography was

configured to map pathways with more than a 30% decrease in anisotropy with a length threshold of 40 mm. The trajectories in Fig. 3a and Fig. 3b are both colored-coded with directional colors (red: left-right green: anterior-posterior blue: superior-inferior). The first row shows tractography viewing from the top, whereas the second rows show from the left. The conventional tractography in Fig. 3a visualizes the trajectories of the entire brain fiber pathways, and there is no gross anomaly visible from the tractography that may suggest a major neurological disorder. This is expected because, at the early stage of multiple sclerosis, the patient usually does not present a gross structural change that can be readily identified in conventional tractography. In comparison, the different tractography in Fig. 3b pinpoints the location of affected pathways in the bilateral primary visual pathway near the visual cortex. The location matches well with the patient's disease presentation of optic neuritis, whereas conventional tractography in Fig. 3a shows no clue to this critical information.

Reliability assessment

We further use patient #1 and a 42-year-old normal subject as the examples to show how the reliability of the differential tractography findings can be quantified using a sham setting. Both the follow-up scans of these two subjects were acquired 6 months after the baseline scans. Figure 4a is the differential tractography of patient #1 and the control subject showing pathways with an increase or decrease anisotropy greater than 30% at different length thresholds (1st row: patient's increase, 2nd row: patient's decrease, 3rd row: normal subject's increase, and 4th row: normal subject's decrease). Only the 2nd row (decreased anisotropy in patient #1) contains possible true findings that imply axonal injury, whereas other rows (1st, 3rd, and 4th) are all false positive results due to either physiological noises (cardiovascular or respiratory) or phase distortion artifact. As shown in Fig. 4a, most false findings at 1st, 3rd, and 4th rows can be effectively removed using a longer length threshold, and there is a trade-off between sensitivity and specificity controlled by the length threshold. A longer length threshold renders a

more specific result with the expense of losing meaningful findings, whereas a shorter length threshold allows for more findings with a risk of taking false results. To quantify the reliability of findings in the 2nd row, we can estimate its FDR by using the total number of findings at the 1st row as an estimate for the number of false findings at the 2nd row. This assumes that the random error will produce a similar number of false findings in the 1st and 2nd row.

Figure 4b and 4c illustrate the FDR calculation. Figure 4b lists the number of findings at different length thresholds and anisotropy thresholds for patient #1 (upper two tables) and the normal subject (lower two tables). It is noteworthy that the "anisotropy threshold" here is the threshold for the decrease of anisotropy quantified by percentage (see Materials and Methods). A threshold of 30% means that the tracking algorithm will track only the fiber orientations with a decrease of anisotropy greater than 30%. The tables on the left are numbers of findings with decreased anisotropy, whereas those on the right are numbers of findings with increased anisotropy. The green colors in the table are those with a larger number of findings, whereas the red colors indicate a smaller number. The tables of the patient show a substantially larger number of findings with decreased anisotropy caused by the disease. In comparison, the two tables of the control subject are substantially similar, and the false results are equally distributed in both tables. We can use the findings with increased anisotropy (the table on the right) to estimate the number of false findings for FDR calculation.

Figure 4c shows the FDR of patient #1's findings calculated using the above-mentioned sham setting. The resulting table shows a trade-off between sensitivity and specificity controlled by both the length threshold and anisotropy threshold. A length threshold of 30~40 mm and an anisotropy threshold at 20~30% decrease of anisotropy provides us an FDR around 0.01, suggesting that around 1% of the tracks shown in the differential tractography are false results. We can use these two thresholds to leverage sensitivity and specificity. For example, lower thresholds are geared toward higher sensitivity to

explore potential neurodegeneration, whereas higher thresholds can provide a confirmatory answer to the axonal damage. The optimal setting can be different based on the disease condition, scan interval, and purposes (e.g. exploratory or confirmatory).

Differential tractography on patients with neurological diseases

We further demonstrate differential tractography in patients with different neurological disorders in Fig. 5 and list the FDR of these findings in Table 2. The scan subjects include patients with MS (#1, #2), HD (#3, #4), ALS (#5), and epilepsy (#6). The first three rows show differential tractography in three views (left sagittal from left, coronal from the front and axial from top) using directional colors, where the last row shows differential tractography with yellow-red colors representing the percentage decrease of anisotropy.

The first notable finding comparing MS patients #1 and #2 is that the volume of affected pathways and their decrease of anisotropy reflect the severity of their clinical symptoms. The medical history of patient #1 (Supplementary Materials) indicates a more severe drop in visual acuity to 20/400 in addition to her visual field defect in all quadrants, while patient #2 only had a decrease of visual acuity to 20/125 with only superior altitudinal visual field defect (Table 1 and Supplementary materials). The greater severity in patient #1 is reflected by a larger volume of affected pathways diffusion (patient #1: 55681.6 mm^3, patient #2: 26124 mm^3) and a greater decrease of anisotropy shown in the last row. This suggests that differential tractography has a quantitative potential to evaluate disease severity using either the volume of affected tracks or the decrease of their anisotropy.

The differential tractography of HD patients #3 and #4 in Fig. 5 both show affected pathways around the stratum. This matches well with the common understanding that striatal pathways are usually involved in Huntington disease. Moreover, the differential tractography in patient #4 has a greater involvement extending to brainstem and cerebellum, suggesting a worse motor performance. This seems to match the patient's medical history of a higher motor score of 64 and her specific dystonia presentation (Table 1 and Supplementary materials).

Patient #5 in Fig. 5 is the differential tractography of an ALS patient. It is noteworthy that the results of this patient are obtained using a 15% decrease threshold because a threshold of 30% yielded no findings. Differential tractography reveals a minor decrease in anisotropy between 15% to 30% in this patient (other cases in Fig. 5 have mostly greater than 30% decrease). This could be explained by the fact that the patient had predominately lower motor neuron symptoms (weakness), and the findings in the central nervous system could be subclinical. Nonetheless, as we lowered the change threshold to 15%, differential tractography showed affected pathways in the right lower corticospinal pathway (blue-purple colored), superior cerebellar peduncle, and posterior corpus callosum, as shown in Fig. 5. The right corticospinal pathway involvement seems to match the patient's history of left side involvement, but it is noteworthy that the FDR of these findings were much higher (FDR~0.2 in Table 2), meaning that around 1/5 of the findings are false positives. The corpus callosum and occipital lobe findings could be subclinical damage and thus did not present any clinical symptoms (discussion in the Discussion section).

Patient #6 was a 51-year-old male with right anterior lobectomy. He was previously an epileptic patient with recurrent epilepsy (medical history in Supplementary materials). The MRI scans were done before the surgery and one year after the surgery. The differential tractography accurately reveals the pathways that were affected by resection of the mesial structures and approximately 5 cm of the anterior temporal

neocortex, illustrating its accurate localization power to detect pathways with neurodegeneration. While the surgical resection only removed part of the temporal gyri, the affected pathways involvement much greater connection networks. Furthermore, the last row shows that the decrease of anisotropy is mostly greater than 50%, indicating a greater axonal loss due to the surgical removal of the brain tissue.

The last column in Fig 5 is the differential tractography of a control. We applied the same settings to examine how differential tractography may capture false results. The differential tractography shows a mild decrease of anisotropy as presented by yellow tracks in the last row, a clue that the change may not be strong enough. Furthermore, there are only 74 findings located at the prefrontal cortex, and the number is substantially smaller than thousands of findings in patients (Table 2). These findings are relatively insignificant compared to those of the patients. Moreover, the location of the findings is known to be heavily affected by the phase distortion artifact, and the findings could be due to the different level of distortion between the repeat scans. However, it is noteworthy that the calculated FDR will be 0 in this case because there are no findings with increase anisotropy for this control subject. This result suggests that the FDR estimation still have its limitation if the number of findings is sufficiently small. The interpretation of differential tractography still needs to consider the percentage decrease of anisotropy, the total number of findings, and possible sources of imaging artifact.

In general, the findings in Fig.5 allows us to quickly differentiates the possible locations of neurodegeneration and evaluate the severity. The affected pathways in MS, HD, and ALS patients show distinctly different topology, allowing for differential diagnosis or prognosis evaluation. Table 2 further shows how we can use the sham setting to calculate the reliability of the results. The FDR indicates the likelihood of a finding in the differential tractography being a false positive.

Discussion

Here we report a novel tractography method to reveal fiber pathways affected by neurodegeneration. We found that differential tractography could serve as a track-based biomarker to provide localization of neurodegeneration and allow for quantifying its severity using the decrease of anisotropy and the total volume of affected pathways. The estimated FDR further offered reliability information to interpret the results, and the findings correlated well with clinical presentations of each individual.

There are several key improvements that make differential tractography a powerful track-based biomarker for individual studies. Diffusion MRI fiber tracking can be viewed as a type of clustering process that is directionally sensitive. Therefore, the tracking-the-difference strategy used in this study is conceptually similar to clustering used in fMRI studies, which groups voxel-wise statistics into clusters to achieve a greater statistical power[21]. By using spatial relations across multiples voxels, the tracking-the-difference strategy has the potential to differentiate true findings from local errors, since neuronal injury will propagate along axonal fibers while local error stays locally. The fiber tracking algorithm visits diffusion metrics along fiber pathways across multiple voxels to present a collective statistic measure. This is a substantial improvement over existing diffusion MRI methods that provide voxel-wise differences for groups studies[18-20].

The advanced MRI acquisitions also played a critical role to boost the sensitivity of differential tractography. The image acquisition used in this study covered a wide range of diffusion sensitization (b-values) and a greater number of diffusion sampling directions. Although we could apply differential tractography to DTI or multi-shell data, our preliminary test (not reported here) on DTI data showed a substantially higher rate of false findings. This is not surprising because a typical DTI acquisition only acquires one b-value of 1,000 mm/s^2 at 30~60 directions, whereas we acquired a range of b-value from

0 to 7,000 mm/s^2 at 257 directions. The early axonal injury seems to affect mostly restricted diffusion and can only be reliably captured if a wider range of b-value is acquired with enough diffusion sampling directions.

It is also noteworthy that the anisotropy used in this study is not the commonly used fractional anisotropy (FA) provided from DTI. FA is a unit-free ratio between 0 and 1 derived from diffusivities that quantify *how fast* water diffuses within the biological tissues. Consequently, FA is an ensemble measurement that will inevitably mix fast and slow diffusion and suffer from partial volume effect. In comparison, the anisotropy in this study quantifies *how much* diffusion is anisotropic. Specifically, it estimates the spin density of restricted anisotropic diffusion at a given diffusion orientation within a given displacement (see Materials and Methods). It is a quantity measurement, and the methodology we used allowed us to separate restricted diffusion from none-restricted diffusion. The differences in biophysical meanings result in different specificity to individual's connectivity patterns[22] and different performance in handling the partial volume effect[15].

Another important result we observed is that differential tractography seems to capture subclinical findings: certain pathways could be damaged without any obvious clinical symptoms reported by patients. For example, the two MS patients shown in Fig. 5 were symptom-free during the follow-up scans after the steroid treatments; however. differential tractography still captures a substantial number of findings related to the primary visual pathways, and the decrease of the anisotropy diffusion correlates well with the severity of the initial clinical presentation. Similarly, by lowering the detection threshold, the ALS patient in Fig. 5 also shows substantial involvement in the posterior corpus callosum that connects to the occipital lobe. Although there is no clinical presentation here supporting our finding, subclinical callosal damage for ALS patients is not uncommon[23], and there are also studies suggested subclinical involvement of occipital lobe in the ALS patients [24,25]. The ability to capture subclinical

findings has a profound clinical implication. It suggests that differential tractography is sensitive enough to provide additional evaluation value on top of existing clinical scales and scores, including expanded disability status scales (EDSS) and patient determined disease steps (PDDS) scales used in MS patients or Unified Huntington's Disease Rating Scale (UHDRS) used in HD patients.

Limitations and possible pitfalls

There are limitations in differential tractography. Differential tractography only works on longitudinal scans of the same subject and only reflects the *change* of anisotropy within the time frame of the repeat scans. It does not access track integrity in a cross-sectional setting. Different tractography may not be able to detect any abnormality if the axonal injury is done at the baseline scans. Further, differential tractography still has false results if the artifact also propagates coincidentally along a fiber pathway. The phase distortion artifact often gives rise to straight lines near the brain surface, but sometime may appear like a spuriously legit connection. Misalignment between baseline and follow-up scans can also generate a false result. The misalignment can happen due to brain tissue shift after surgical intervention or more commonly the registration error. It will artificially create mirrored findings in both the increase and decrease of anisotropy along the misaligned pathways.

There are still other possible causes of false results. The subjects may have substantial movement in the follow-up scan, but not in the study or sham scan. There may be inconsistency in image acquisition between repeat scans such as changing the head coils or scanning protocol. Both scenarios can produce spurious findings, and thus a series of quality control is always needed to avoid these getting false results. Furthermore, the findings in differential tractography still need to be examined under neuroanatomy. Spurious findings often appear near the brain surface with odd trajectories (straight

lines), while true findings tend to follow the trajectories of well-known neuroanatomical pathways. Prior neuroanatomy knowledge may help exclude false results from true findings.

Clinical applications

Differential tractography can be used in differential diagnosis and evaluation of a treatment or intervention. Neurologists can use it for differential diagnosis as patients with different neurological disorders will present distinctly different spatial patterns in their affected pathways. The location will provide a clue about the possible causes to resolve difficult clinical cases. This is otherwise not achievable in structural MRI unless a gross lesion or atrophy is visible in the late stage of neurodegeneration. Another application of differential tractography is for evaluating an intervention or treatment. Differential tractography can provide an objective quantitation that is directly comparable across subjects and less susceptible to observer differences. It could minimize variance due to evaluator differences and increase effect size in comparison with the conventional evaluation conducted by patients or neurologists. This opens a gate for early treatments to restore subclinical injuries before those injuries accumulate to become a major functional deficit.

Materials and Methods

MRI experiments on clinical patients with neurological disorders

The diffusion MRI acquisition included a baseline scan and another follow-up scan (acquired months later) of the same subject. We acquired scans on 6 patients with different neurological diseases including multiple sclerosis, Huntington disease, ALS, and epilepsy. Table 1 summarizes their basic demographic and scan interval information, and brief medical history of these patients are summarized

in Supplementary Materials. The ALS patient was previously reported[26]. Each diffusion MRI scan acquired 22 b-values ranging from 0 to 7,000 s/mm^2 at a total of 257 diffusion sampling direction using a q-space imaging scheme[27]. The in-plane resolution and slice thickness were 2.4 mm. TE=154 ms, and TR=9500 ms.

Quality control of diffusion MRI data

We applied a series of quality control to our diffusion weighted image data to minimize possible false results due to acquisition issues. The first quality control was done by checking whether the image dimension, resolution, and b-table were consistent between repeat scans. All scan data were confirmed to have a consistent setting between repeat scans. The second quality control was done by calculating the mean Pearson correlation coefficient of the neighboring diffusion-weighted images:

$$\frac{1}{n}\sum_{i=1}^{n}\rho\left(S_i, S_{N(i)}\right) \quad (1)$$

where ρ calculates the Pearson correlation coefficient, S_i is the *i*-th diffusion weighted image, and $N(i)$ returns the index of another diffusion weighted image acquired by the most similar diffusion sensitization in the q-space:

$$N(i) = arg\min_{j,j\neq i}\left\|\sqrt{b(i)}\vec{g}(i) - \sqrt{b(j)}\vec{g}(j)\right\| \quad (2)$$

$b(i)$ is the b-value, and $\vec{g}(i)$ is the diffusion encoding direction. The resulting values in Eq. (1) ranges between 0.6~0.8, and a data set would be rejected if the baseline and follow-up scans have a difference in mean Pearson correlation coefficient greater than 0.1. In this study, one ALS patient's data we recruited previously[26] was rejected because the baseline scan had a substantially lower value due to slice shift during the scan.

The third quality control step was identifying slice-wise signal dropout for each slice in each diffusion-weighted image. This examination excluded slices with a large background region (defined by the brain mask), which is greater than 15/16 of the entire slice area. For each slice, we calculated its Pearson correlation coefficients with four of its signal-related slices, including its upper neighboring slice, lower neighboring slice, and the same-location slices of two neighboring diffusion-weighted images. The maximum of these four correlation values was used as the representative correlation coefficient of the slice under examination, and a signal dropout would result in a decrease of this representative correlation coefficient. If a slice had an average decrease of representative correlation coefficient greater than 0.1 in comparison with its four related slices, we identified it as a signal dropout slice. In this study, we accepted the data set if the number of signal dropout slices was smaller than 0.1% of the total slice number (i.e. < 25 slices). All data set were screened and passed this criterion.

The fourth quality control was checking the b-table orientation using the fiber coherence index[32]. One scan was found to have slices order flipped upside down. The data were corrected before further analysis.

After the quality control steps, the diffusion data of the follow-up scans were compared with baseline scans using the following analysis:

Empirical Distribution of Water Diffusion

The empirical distribution of water diffusion was calculated from diffusion-weighted signals using generalized q-sampling imaging (GQI)[28]. This “empirical distribution” has no assumption of the underlying distribution (e.g. Gaussian distribution), and thus it can be applied to a variety of fiber or biological conditions. The empirical distribution calculated from GQI, termed spin distribution function

(SDF), has a different physical definition from the *diffusivity* calculated from DTI that quantifies how fast the diffusion is. The SDF quantifies the *density* of restricted diffusion sampled at any orientations, and it can be calculated using the formula:

$$\Psi_0(\boldsymbol{r},\hat{u}) = Z_0 \sum_i W_0(\boldsymbol{r},i)\, sinc\left(\sigma\sqrt{6D\mathrm{b}(i)}\langle\hat{\mathrm{g}}(i),\hat{\mathrm{u}}\rangle\right) \qquad (3)$$

$\Psi_0(\boldsymbol{r},\hat{u})$ is the SDF value oriented at $\hat{u}$ and sampled from a voxel located at ***r***. Z_0 is a scaling constant to convert the arbitrary unit of the diffusion signals to a density unit. i iterates through each diffusion weighted signals $\mathrm{W}(\boldsymbol{r},\mathrm{i})$, and $\mathrm{b}(\mathrm{i})$ is the b-value, $\hat{\mathrm{g}}(\mathrm{i})$ is the direction of the diffusion sensitization gradient. σ is the diffusion sampling ratio controlling the displacement range of the diffusing spins. *D* is the diffusivity of free water at room temperature.

We further need to calculate SDFs of the follow-up scan and transformed them into the space of the baseline scan (Fig. 1a and Fig. 1b) so that they could be directly compared. This was done using q-space diffeomorphic reconstruction (QSDR)[29], a method that generalizes GQI to accept spatial transformation in the reconstruction. QSDR allows us to simultaneously reconstruct and transform SDF from the space of the follow-up scan to the space of the baseline scan using the following formula:

$$\Psi_1(\boldsymbol{r},\hat{u}) = Z_1 \sum_i W_1(\phi(\boldsymbol{r}),i) sinc\left(\sigma\sqrt{6Db(i)}\langle\hat{g}(i),\mathbf{J}(\boldsymbol{r})\hat{u}\rangle\right) \qquad (4)$$

where $\phi(\boldsymbol{r})$ transforms spatial coordinate ***r*** from the space of the baseline scan to that of follow-up scan. Since the scans are from the same subject, we assume there is only “rigid body” transformation (i.e. only rotation or translocation) between the scans. Please note that this assumption can be violated if there is a large tissue distortion due to edema or tissue removal. To handle this condition, a nonlinear spatial registration can be used in QSDR. For rigid body transformation, the computation is a simple matrix-vector multiplication. The rigid body transformation matrix can be obtained by linear registering

the b0 images (or the sum of all diffusion weighted images). We used the correlation coefficient between the images from baseline and follow-up scans as a cost function to calculate the transformation matrix. The cost function was minimized using a gradient descent method. $W_1(\phi(\boldsymbol{r}), i)$ is the diffusion weighted signals at coordinate $\phi(\boldsymbol{r})$. $\mathbf{J}(\boldsymbol{r})$ is the Jacobian matrix at the same coordinate that rotates the unit vector $\hat{u}$. Here the Jacobian matrix is the rotation matrix of the rigid body transformation. There other variables follow the same notations in Eq. (3). Please note that the SDFs calculated from Eq. (3) and (4) have "arbitrary units". Therefore, the Z_1 constant in Eq. (4) need to be scaled to match the same unit of Z_0 in Eq. (3). This signal matching can be done using the sum of all diffusion weighted images from two scans:

$$Z_1 = Z_0 \frac{\sum_r W_1(\phi(\boldsymbol{r}),0)}{\sum_r W_0(\boldsymbol{r},0)} \quad (5)$$

The isotropic component of an SDF is then removed by subtracting its minimum values.

$$\Psi_0'(\boldsymbol{r},\hat{u}) = \Psi_0(\boldsymbol{r},\hat{u}) - \min_{\hat{u}} \Psi_0(\boldsymbol{r},\hat{u}) \quad (6)$$

$$\Psi_1'(\boldsymbol{r},\hat{u}) = \Psi_1(\boldsymbol{r},\hat{u}) - \min_{\hat{u}} \Psi_1(\boldsymbol{r},\hat{u}) \quad (7)$$

This approach obtains the "anisotropic SDF" (termed anisotropy hereafter) and minimizes the effect of free water diffusion[15]. It is noteworthy that this anisotropy measurement has a different physical meaning from the fractional anisotropy (FA) calculated in DTI. FA is a ratio ranged between 0 and 1. It is calculated from diffusivities and has no unit. In comparison, the anisotropy quantified in this study is calculated from the SDF and has the same unit of the SDF, which is the density of diffusing water in the arbitrary unit.

Tracking Differences in the SDF

To track differences in the SDF, we first determined the local fiber orientations using the peaks on the sum of $\Psi_0(\boldsymbol{r},\hat{u})$ and $\Psi_1(\boldsymbol{r},\hat{u})$ to guide a deterministic fiber tracking algorithm[15]. Then we calculated the percentage difference in the anisotropy between baseline and follow-up scans (Fig. 1c):

$$\Psi_d(\boldsymbol{r},\hat{u}) = \frac{2\left(\Psi_1{}'(\boldsymbol{r},\hat{u}) - \Psi_0{}'(\boldsymbol{r},\hat{u})\right)}{\Psi_1{}'(\boldsymbol{r},\hat{u}) + \Psi_0{}'(\boldsymbol{r},\hat{u})} \times 100\% \qquad (8)$$

The percentage changes in the anisotropy, $\Psi_d(\boldsymbol{r},\hat{u})$, can have positive values (blue SDFs in Fig. 1c), which indicates an increase in the density of anisotropic diffusion, or negative values (red SDFs in Fig. 1c), which indicates a decrease in the density of anisotropic diffusion. Then we added an additional criterion to the algorithm to track fiber directions with a decrease or an increase in the anisotropy greater than a percentage threshold, respectively. To track fiber directions with an increase of anisotropy, the additional criterion checked whether the increase of anisotropy is greater than a predefined value (e.g. 20%) and continue tracking as long as the criterion is satisfied:

$$\Psi_d(\boldsymbol{r},\hat{a}) > \theta^+ \qquad (9)$$

where $\hat{a}$ is the local fiber directions used in the fiber tracking algorithm. Similarly, to track pathways with decreased anisotropy, the criteria continues tracking if the decrease of anisotropy is greater than a predefined percentage (e.g. -20%):

$$\Psi_d(\boldsymbol{r},\hat{a}) < \theta^- \qquad (10)$$

This allows us to track two different sets of pathways, one for increased anisotropy, one for decreased anisotropy. The other criteria follow the default settings in the generalized deterministic fiber tracking algorithm (e.g. seeding strategy, propagation interval, angular threshold, length constraint…etc.)[15],

which has been shown to achieve high accuracy in regular tractography in an open competition (#ID 03)[30].

The differential tractography was then obtained by placing a total of 5,000,000 seeding points in the white matter. Two iterations of topology-informed pruning[31] were applied to the tractography to remove noisy findings. Track with lengths shorter than the length threshold was discarded, and the results of different length threshold were compared to access its effect on the sensitivity and specificity of differential tractography.

Estimating false discovery rate using a sham setting

Figure 6 showed the experiment design that allows for estimating positive predictive value (FDR) of differential tractography in individual scans. The baseline scan (Fig. 6a) is compared with the follow-up scan (Fig. 6b upper row) using differential tractography to reveal tracks with decreased anisotropic SDF (Fig. 6c, upper row). Differential tracking was conducted to track pathways with decreased anisotropy. A total of 5,000,000 iterations were conducted, starting from 5,000,000 different seeding points in the white matter and tracking in two directions. Here we viewed each tracking iteration as a hypothesis test since each tracking iteration was done independently. The null hypothesis is “there exists no track with a decrease in the anisotropy”, which means “track length = 0”. We rejected this hypothesis if the track length from differential tracking was greater than a predefined length threshold (e.g. 40 mm). Each rejected hypothesis is thus regarded as a “positive findings”, and it can be either a true positive or false positive.

As shown by the example in the upper row of Fig. 6c, the number of tracks with affected tracks longer than 40 mm is 3921, meaning that we reject 3921 null hypotheses and get 3921 total positive findings. Those finding includes both true positive and false positive findings. To estimate the number of false

positive findings, a sham scan can be acquired on the same day of the baseline scan (Fig. 6b, lower row), and thus any positive findings shown in the sham scan should be false positive findings. The same tracking process is applied to track from the same 10,000 seeding point. The example in the lower of Fig. 6c shows, the sham scan generates a total of 45 tracks with a length greater than 40 mm, meaning that the estimated number of false positive findings is 45. Using this information, we can calculate the false discovery rate (FDR)(i.e. 45/3921) and the FDR (i.e. 1-45/3921, as shown in Fig. 6d) of this individual scan.

In this study, we did not acquire additional sham scan, and an alternative approach was used. Since there should be no increased track integrity during the disease course, any findings showing *increased* anisotropy can be regarded as false positive findings. Therefore, we can use the number of tracks with *increased* anisotropy in the follow-up scan as a substitute sham scan. Even if tracks with increased connectivity do exist due to rehabilitation or treatment, it will increase our estimated number of false positive findings and lower our positive predictive value. This means that the FDR estimated by this alternative approach will be a lower bound of the actual FDR and can be a conservative estimate of FDR. This minimized the chance that we overestimate the reliability of findings in differential tractography.

The processing pipeline for differential tractography and the quality control procedure is implemented in DSI Studio (http://dsi-studio.labsolver.org). Documentation and source code are also available on the same website.

Acknowledgments

Research reported in this publication/press release was partly supported by NIMH of the National Institutes of Health under award number R56MH113634. The content is solely the responsibility of the authors and does not necessarily represent the official views of the National Institutes of Health. The MRI scans were partly supported by the Walter L. Copeland Fund of The Pittsburgh Foundation.

References

1 Wattjes, M. P. *et al.* Evidence-based guidelines: MAGNIMS consensus guidelines on the use of MRI in multiple sclerosis--establishing disease prognosis and monitoring patients. *Nat Rev Neurol* **11**, 597-606, doi:10.1038/nrneurol.2015.157 (2015).

2 Rovira, A. *et al.* Evidence-based guidelines: MAGNIMS consensus guidelines on the use of MRI in multiple sclerosis-clinical implementation in the diagnostic process. *Nat Rev Neurol* **11**, 471-482, doi:10.1038/nrneurol.2015.106 (2015).

3 Tabrizi, S. J. *et al.* Potential endpoints for clinical trials in premanifest and early Huntington's disease in the TRACK-HD study: analysis of 24 month observational data. *Lancet Neurol* **11**, 42-53, doi:10.1016/S1474-4422(11)70263-0 (2012).

4 Tabrizi, S. J. *et al.* Biological and clinical manifestations of Huntington's disease in the longitudinal TRACK-HD study: cross-sectional analysis of baseline data. *Lancet Neurol* **8**, 791-801, doi:10.1016/S1474-4422(09)70170-X (2009).

5 Basser, P. J., Mattiello, J. & LeBihan, D. Estimation of the effective self-diffusion tensor from the NMR spin echo. *J Magn Reson B* **103**, 247-254 (1994).

6 Song, S. K. *et al.* Demyelination increases radial diffusivity in corpus callosum of mouse brain. *Neuroimage* **26**, 132-140, doi:S1053-8119(05)00022-4 [pii]

10.1016/j.neuroimage.2005.01.028 (2005).

7 Song, S. K. *et al.* Dysmyelination revealed through MRI as increased radial (but unchanged axial) diffusion of water. *Neuroimage* **17**, 1429-1436, doi:S105381190291267X [pii] (2002).

8 Huisman, T. A. *et al.* Diffusion tensor imaging as potential biomarker of white matter injury in diffuse axonal injury. *AJNR Am J Neuroradiol* **25**, 370-376 (2004).

9 Werring, D. J. *et al.* Diffusion tensor imaging can detect and quantify corticospinal tract degeneration after stroke. *J Neurol Neurosurg Psychiatry* **69**, 269-272 (2000).

10 Werring, D. J., Clark, C. A., Barker, G. J., Thompson, A. J. & Miller, D. H. Diffusion tensor imaging of lesions and normal-appearing white matter in multiple sclerosis. *Neurology* **52**, 1626-1632 (1999).

11 Budde, M. D., Xie, M., Cross, A. H. & Song, S. K. Axial diffusivity is the primary correlate of axonal injury in the experimental autoimmune encephalomyelitis spinal cord: a quantitative pixelwise analysis. *J Neurosci* **29**, 2805-2813, doi:29/9/2805 [pii]

10.1523/JNEUROSCI.4605-08.2009 (2009).

12 Wang, Y. *et al.* Quantification of increased cellularity during inflammatory demyelination. *Brain* **134**, 3590-3601, doi:10.1093/brain/awr307

awr307 [pii] (2011).

13 Henf, J., Grothe, M. J., Brueggen, K., Teipel, S. & Dyrba, M. Mean diffusivity in cortical gray matter in Alzheimer's disease: The importance of partial volume correction. *Neuroimage Clin* **17**, 579-586, doi:10.1016/j.nicl.2017.10.005 (2018).

14 Melonakos, E. D. *et al.* Voxel-based morphometry (VBM) studies in schizophrenia-can white matter changes be reliably detected with VBM? *Psychiatry Res* **193**, 65-70, doi:S0925-4927(11)00037-0 [pii]

10.1016/j.pscychresns.2011.01.009 (2011).

15 Yeh, F. C., Verstynen, T. D., Wang, Y., Fernandez-Miranda, J. C. & Tseng, W. Y. Deterministic diffusion fiber tracking improved by quantitative anisotropy. *PLoS ONE* **8**, e80713, doi:10.1371/journal.pone.0080713

PONE-D-13-26801 [pii] (2013).

16 Wedeen, V. J. *et al.* The geometric structure of the brain fiber pathways. *Science* **335**, 1628-1634, doi:335/6076/1628 [pii]

10.1126/science.1215280 (2012).

17 Glasser, M. F. *et al.* The Human Connectome Project's neuroimaging approach. *Nat Neurosci* **19**, 1175-1187, doi:10.1038/nn.4361 (2016).

18 Sanchez-Castaneda, C. *et al.* Seeking Huntington disease biomarkers by multimodal, cross-sectional basal ganglia imaging. *Hum Brain Mapp* **34**, 1625-1635, doi:10.1002/hbm.22019 (2013).

19 Roosendaal, S. D. *et al.* Regional DTI differences in multiple sclerosis patients. *Neuroimage* **44**, 1397-1403, doi:10.1016/j.neuroimage.2008.10.026 (2009).

20 Sydykova, D. *et al.* Fiber connections between the cerebral cortex and the corpus callosum in Alzheimer's disease: a diffusion tensor imaging and voxel-based morphometry study. *Cereb Cortex* **17**, 2276-2282, doi:10.1093/cercor/bhl136 (2007).

21 Woo, C. W., Krishnan, A. & Wager, T. D. Cluster-extent based thresholding in fMRI analyses: pitfalls and recommendations. *Neuroimage* **91**, 412-419, doi:10.1016/j.neuroimage.2013.12.058 (2014).

22 Yeh, F. C. *et al.* Quantifying Differences and Similarities in Whole-Brain White Matter Architecture Using Local Connectome Fingerprints. *PLoS Comput Biol* **12**, e1005203, doi:10.1371/journal.pcbi.1005203 (2016).

23 Filippini, N. *et al.* Corpus callosum involvement is a consistent feature of amyotrophic lateral sclerosis. *Neurology* **75**, 1645-1652, doi:10.1212/WNL.0b013e3181fb84d1 (2010).

24 Zhang, Y. *et al.* Occipital cortical gyrification reductions associate with decreased functional connectivity in amyotrophic lateral sclerosis. *Brain Imaging Behav* **11**, 1-7, doi:10.1007/s11682-015-9499-9 (2017).

25 Loewe, K. *et al.* Widespread temporo-occipital lobe dysfunction in amyotrophic lateral sclerosis. *Sci Rep* **7**, 40252, doi:10.1038/srep40252 (2017).

26 Abhinav, K. *et al.* Use of diffusion spectrum imaging in preliminary longitudinal evaluation of amyotrophic lateral sclerosis: development of an imaging biomarker. *Front Hum Neurosci* **8**, 270, doi:10.3389/fnhum.2014.00270 (2014).

27 Callaghan, P. T. *Principles of Nuclear Magnetic Resonance Microscopy*. (Oxford University Press, 1991).

28 Yeh, F. C., Wedeen, V. J. & Tseng, W. Y. Generalized q-sampling imaging. *IEEE Trans Med Imaging* **29**, 1626-1635, doi:10.1109/TMI.2010.2045126 (2010).

29 Yeh, F. C. & Tseng, W. Y. NTU-90: a high angular resolution brain atlas constructed by q-space diffeomorphic reconstruction. *Neuroimage* **58**, 91-99, doi:S1053-8119(11)00639-2 [pii]

10.1016/j.neuroimage.2011.06.021 (2011).

30 Maier-Hein, K. H. *et al.* The challenge of mapping the human connectome based on diffusion tractography. *Nat Commun* **8**, 1349, doi:10.1038/s41467-017-01285-x (2017).

31 Yeh, F. C. *et al.* Automatic Removal of False Connections in Diffusion MRI Tractography Using Topology-Informed Pruning (TIP). *Neurotherapeutics*, doi:10.1007/s13311-018-0663-y (2018).

32 Schilling, K. G. *et al.* A fiber coherence index for quality control of B-table orientation in diffusion MRI scans. *Magn Reson Imaging* **58**, 82-89, doi:10.1016/j.mri.2019.01.018 (2019).

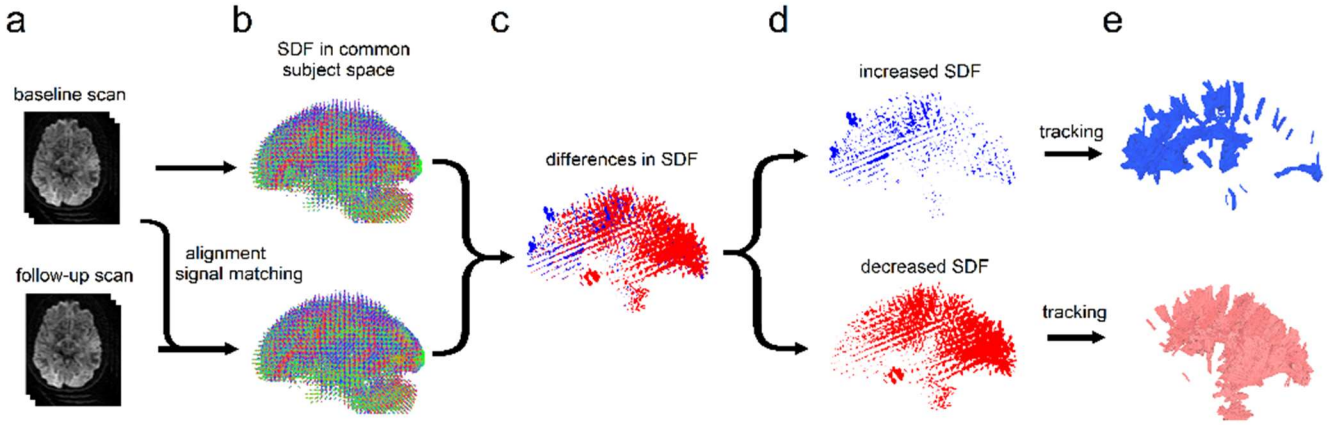

Fig. 1 The flow chart of differential tractography. (a) The baseline and follow-up scans of the same subject are spatially aligned, and the diffusion signals are scaled to the same unit. (b) The spin distribution function (SDF) from two scans are reconstructed in the same common subject space. (c) The differences in SDF are computed for each voxel. (d) Increased and decreased SDF values are separated to guide a “tracking-the-difference” algorithm. (e) The differential tractography shows tracks with increased and decreased anisotropy, respectively. The tracks with decreased anisotropy suggest possible neurodegeneration, whereas the number of tracks with increased anisotropy can be used to estimate the number of false findings.

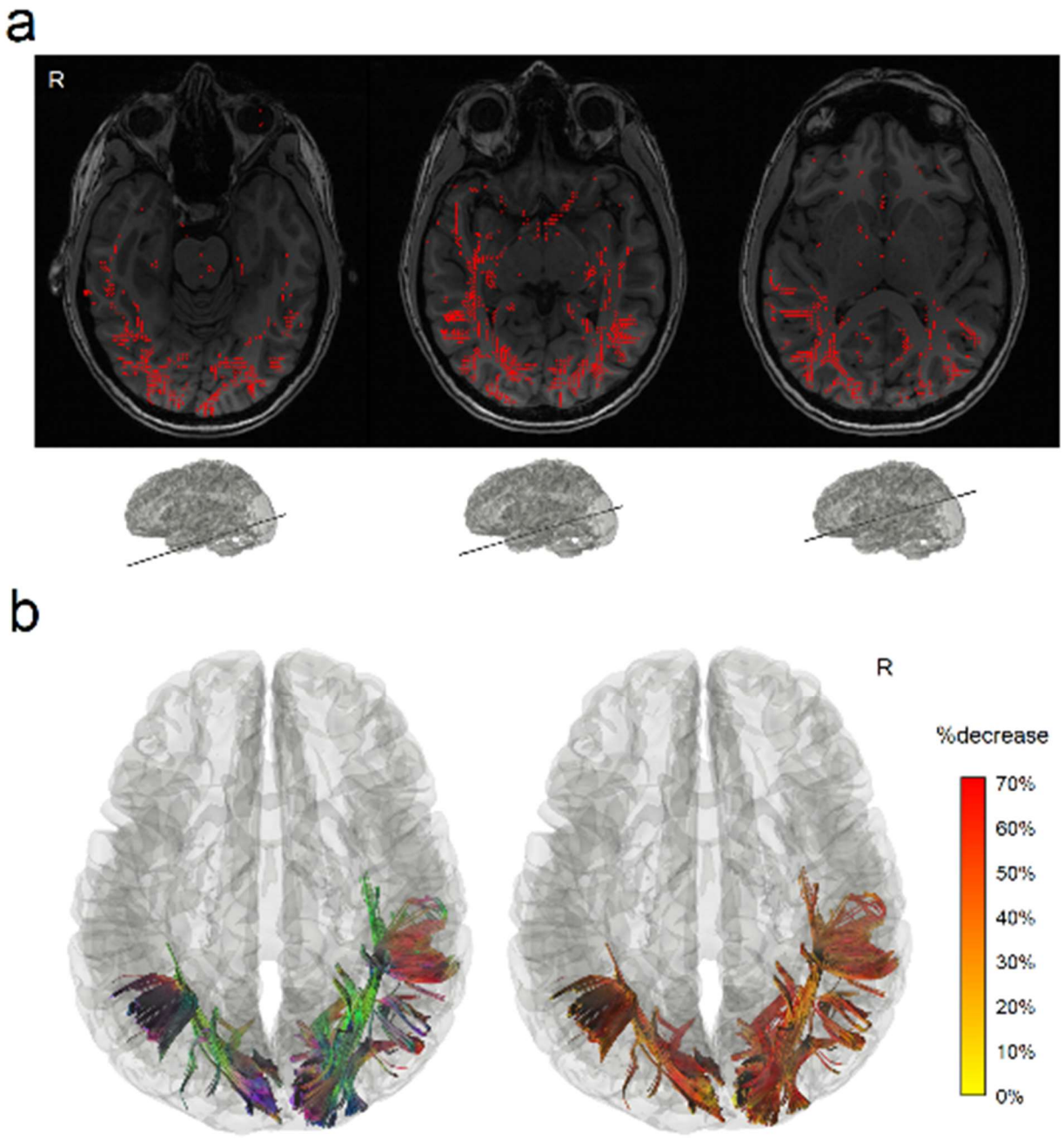

Fig. 2 Differential tractography of a multiple sclerosis patient with the first episode of optic neuritis. (a) The intermediate result of differential tractography shows voxel-wise red sticks indicating local fiber orientations with a substantial decrease in anisotropy (>30%) between repeat scans. The sticks are mostly distributed along the primary visual pathways, while sporadic false findings can also be found

throughout the entire whiter matter regions due to local signal variations. (b) The red sticks are tracked and connected into continuous trajectories, whereas the other unaffected parts of the white matter pathways are ignored. The resulting tractography is the differential tractography of the patient showing the exact segment of pathways with a substantial decrease in anisotropy. The tractography can be rendered by directional colors (left) or severity-coded color (right) to provide information about the spatial location and the severity of the axonal damage quantified by percentage decrease of anisotropic diffusion.

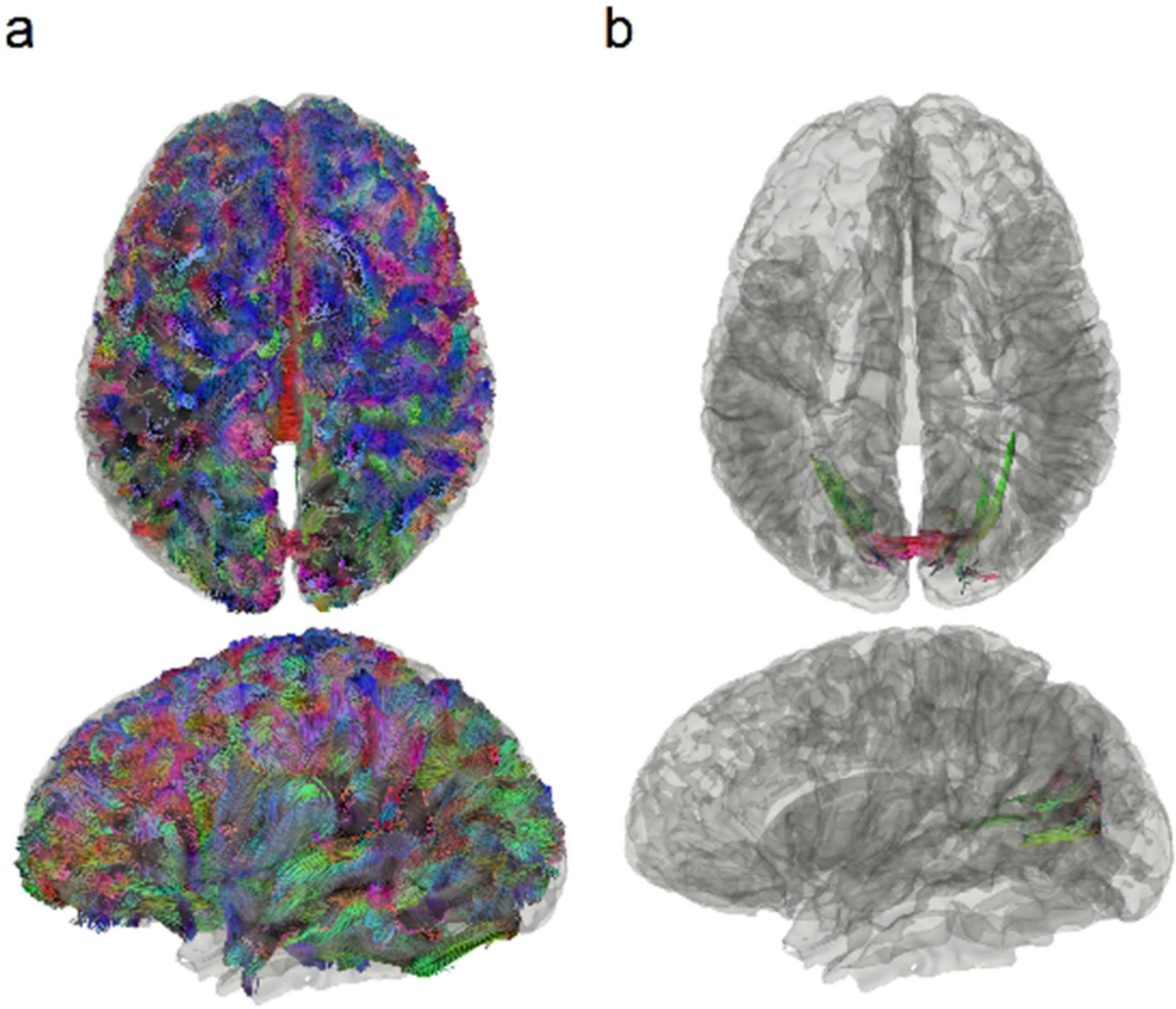

Fig. 3 Conventional tractography compared with differential tractography using the same data from a multiple sclerosis patient with the first episode of optic neuritis. (a) Conventional tractography shows all existing fiber pathways in the human brain and is insensitive to a decrease in the anisotropy. (b) Differential tractography ignores unaffected regions and shows the exact segments of the pathways that have a substantial decrease of anisotropy quantified between repeat scans of the same individual.

a

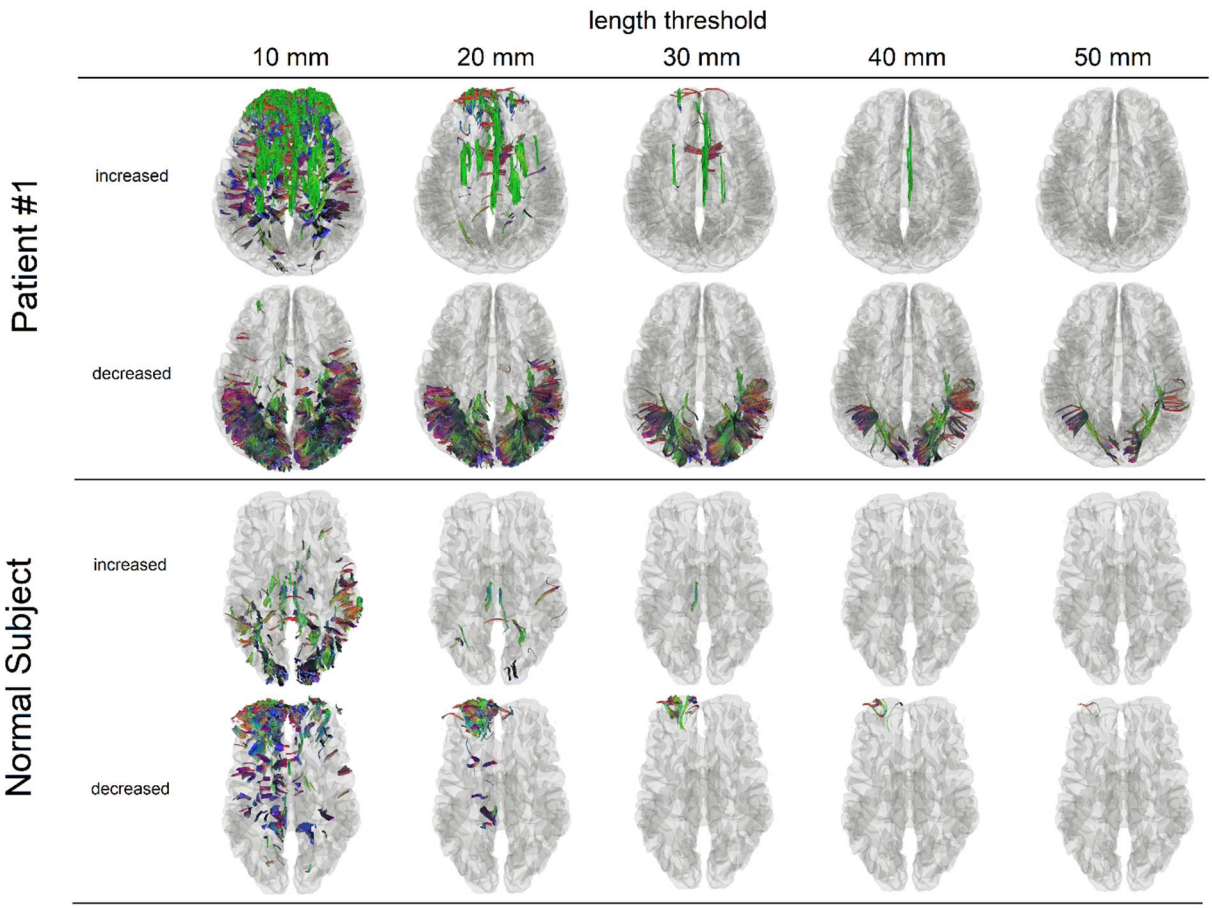

b

Decreased anisotropic diffusion

Total number of findings

percentage change \ length threshold	5 mm	10 mm	15 mm	20 mm	25 mm	30 mm	35 mm	40 mm	45 mm	50 mm
Patient #1										
5%	1741351	1300872	1029189	831543	658570	520201	412292	329956	271372	225089
10%	1429684	1044424	807590	628371	471814	352945	271835	217209	174196	137401
15%	1168368	838584	624868	460072	329969	241255	178898	137548	103219	74672
20%	950089	656779	485535	313947	208803	141978	95553	66748	46647	32114
25%	762423	500475	330589	207117	129843	78743	49219	29778	18507	10984
30%	594279	365921	227000	130699	74278	41314	24037	13947	8954	5591
35%	458383	268452	155041	79726	41191	22615	12313	6833	4070	2594
40%	351789	196122	104130	48019	22157	12484	7184	3869	2138	1352
45%	264008	134665	65426	27725	12841	6774	3717	1731	1097	938
50%	193721	86867	37127	13945	5719	2788	1707	1094	867	373

Total number of findings

percentage change \ length threshold	5 mm	10 mm	15 mm	20 mm	25 mm	30 mm	35 mm	40 mm	45 mm	50 mm
Normal Subject										
5%	1532540	1016007	736587	558480	410705	296163	214446	152840	113967	89654
10%	1116921	677778	458382	318191	203417	135969	97257	70070	52043	39166
15%	783570	430102	253608	152045	84398	52312	33528	20284	11175	6921
20%	529059	249001	121623	61641	29242	15123	7843	3816	1659	721
25%	339743	127212	49119	17178	5080	2033	745	221	10	0
30%	210852	62904	18240	5355	1265	658	205	74	15	4
35%	129556	31810	6851	1219	45	0	0	0	0	0
40%	81132	16449	2388	227	12	0	0	0	0	0
45%	50325	8999	1275	117	1	0	0	0	0	0
50%	32830	5641	894	118	1	0	0	0	0	0

Increased anisotropic diffusion

Number of false findings

percentage change \ length threshold	5 mm	10 mm	15 mm	20 mm	25 mm	30 mm	35 mm	40 mm	45 mm	50 mm
5%	1381594	703425	360475	190629	105488	61058	38425	19696	11831	7573
10%	1079172	455140	188654	76000	30831	14084	7436	2983	1276	436
15%	857968	306406	104296	34730	13515	5866	2617	957	211	41
20%	702804	219249	61391	18232	7923	3951	1330	254	102	41
25%	598535	168046	41284	12935	6016	2899	899	182	74	0
30%	520737	131945	30455	10937	4411	1561	561	177	74	0
35%	459015	105249	23301	9586	3690	1195	515	178	75	0
40%	410224	88807	20004	8615	3340	1149	492	177	74	0
45%	371508	78656	17451	8095	2979	968	453	177	72	0
50%	341052	68815	15952	7345	2713	942	452	174	72	0

Total number of findings

percentage change \ length threshold	5 mm	10 mm	15 mm	20 mm	25 mm	30 mm	35 mm	40 mm	45 mm	50 mm
5%	1281383	823239	574970	419083	307132	228994	170807	124465	91894	65932
10%	928467	525367	325643	213085	139864	95854	65026	41830	27406	18643
15%	629964	300491	155428	85871	44823	25127	11988	5308	3081	1604
20%	405201	157045	61802	24555	9640	4336	493	77	0	0
25%	249889	77196	23754	8015	2868	959	195	42	0	0
30%	152774	39719	10629	2883	1332	521	30	0	0	0
35%	93626	19813	5138	1275	752	368	4	0	0	0
40%	57891	10915	3040	1068	633	58	0	0	0	0
45%	33400	5331	1469	680	326	0	0	0	0	0
50%	21692	3406	1074	549	132	0	0	0	0	0

c

False discovery rate (FDR)

percentage change \ length threshold	5 mm	10 mm	15 mm	20 mm	25 mm	30 mm	35 mm	40 mm	45 mm	50 mm
5%	0.7934	0.54073	0.35025	0.22925	0.16018	0.11737	0.0932	0.05969	0.0436	0.03364
10%	0.75483	0.43578	0.2336	0.12095	0.06535	0.0399	0.02735	0.01373	0.00733	0.00317
15%	0.73433	0.36538	0.16691	0.07549	0.04096	0.02431	0.01483	0.00696	0.00204	0.00055
20%	0.73972	0.33382	0.13187	0.05807	0.03798	0.02783	0.01392	0.00381	0.00219	0.00128
25%	0.78504	0.33577	0.12488	0.06245	0.04633	0.03682	0.01827	0.00611	0.004	0
30%	0.87625	0.36058	0.13416	0.08368	0.05939	0.03778	0.02334	0.01269	0.00826	0
35%	1	0.39206	0.15029	0.12024	0.08958	0.05284	0.04183	0.02605	0.01843	0
40%	1	0.45282	0.19211	0.17941	0.15074	0.09204	0.06849	0.04575	0.03461	0
45%	1	0.58409	0.26673	0.29197	0.23199	0.1429	0.12187	0.10225	0.06563	0
50%	1	0.79219	0.42966	0.52671	0.47438	0.33788	0.26479	0.15905	0.08304	0

Fig. 4 Reliability assessment of differential tractography using the length threshold. (a) Differential tractography is applied to a multiple sclerosis patient and a normal subject at different length thresholds. Only the tracks with decreased anisotropy in patient #1 may contain true positive findings, whereas tracks with increased anisotropy in patient #1 or any tracks in the normal subject are false positives for neurodegeneration. A longer length threshold (e.g. > 40mm) can reduce false findings at the expense of sensitivity, whereas a shorter threshold may introduce more false results. (b) The numbers of findings at different length thresholds and anisotropy thresholds are listed in tables. The patient has substantially large numbers of tracks with decreased anisotropy, suggesting a possible neurological injury. In comparison, the normal subject has similar numbers of tracks with increased and decreased anisotropy. (c) False discovery rate (FDR) of the findings in a patient can be calculated by using the patient's own numbers of tracks with increased anisotropy as an estimation of the number of false findings. This allows for adjusting the sensitivity and specificity of differential tractography and quantifying the reliability at different length and anisotropy thresholds.

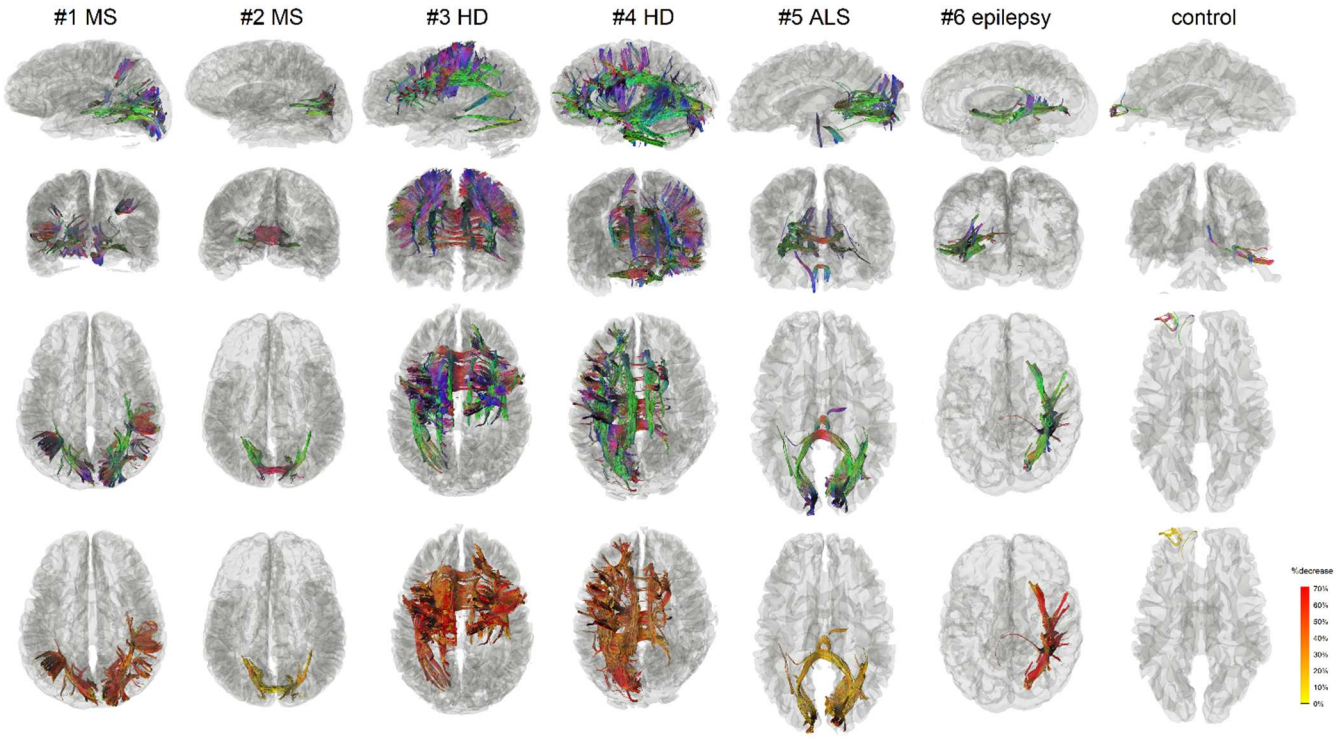

Fig. 5 Differential tractography of patients with different neurological disorders in comparison with a normal subject. The results were generated automatically without expert selection. The differential tractography of the two MS patients matches well with their clinical presentation of optic neuritis. Patient #1 has a much severer drop in visual acuity, which can be quantitatively reflected by her larger the volume of the findings and a greater percentage decrease of the anisotropy along the affected pathways. The differential tractography of the two Huntington diseases shows extensive affected striatal pathways. Patient #4 had more asymmetric dystonia, matching the asymmetry presentation of the differential tractography. The ALS patient had lower motor neuron presentation of left-hand weakness, matching the finding of right lower corticospinal pathways in differential tractography. The epileptic patients received right anterior temporal lobectomy, matching the findings in differential tractography that shows the affected pathways around the surgical location. The false findings in the normal subject can be

differentiated by a much less decrease of anisotropy and its location at the anterior frontal region that is known to be more susceptible to phase distortion artifact.

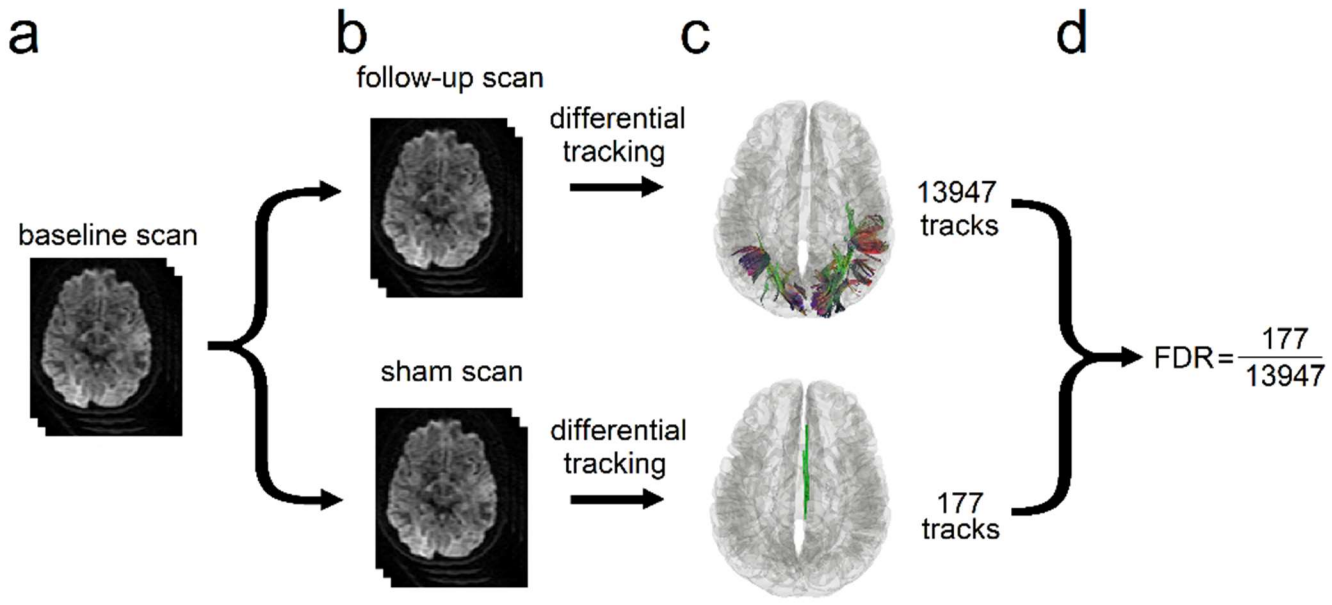

Fig. 6 Diagram showing the sham setting for calculating the false discovery rate (FDR). The baseline scan (a) is compared with a follow-up scan (upper row) and a sham scan (lower row) to generate findings. The follow-up scan is often acquired months after the baseline to capture the decrease of anisotropy diffusion, whereas the sham setting can be a repeat scan on the same day or the findings with increased anisotropy in the follow-up scans. (c) the number of findings from the sham setting (lower row) is used to estimate the number of false findings and to calculate FDR (d).

Table 1: Patient demographics and major symptoms

	diagnosis	age	sex	MRI scans	Major symptoms
#1	multiple sclerosis	44	F	onset of symptom and 6-month follow-up	acute onset of left ocular pain, pain with eye movements, blurring vision of the left eye (20/400), loss of visual field in all quadrants.
#2	multiple sclerosis	24	F	onset of symptom and 6-month follow-up	acute onset of left ocular pain, pain with eye movements, blurring vision of the right eye (20/125), superior altitudinal visual field defect.
#3	Huntington disease	60	M	two scans at 5 months apart during the manifest stage	body bradykinesia on both sides UHDRS motor: 45→49 (worsening)
#4	Huntington disease	55	F	two scans at 5 months apart during the manifest stage	dystonia of left upper extremity, dragging right foot with ambulation, dystonia of the right leg UHDRS motor: 53→64 (worsening)
#5	amyotrophic lateral sclerosis	48	M	baseline scan acquired 30 months after onset follow-up scan acquired one year after.	left-hand weakness with fasciculations ALSFRS-R: 45→32 (worsening)
#6	epilepsy	51	M	before anterior temporal lobectomy and one-year follow-up after surgery	

Table 2: False Discovery Rate of Differential Tractography Findings

	diagnosis	anisotropy threshold	length threshold	number of findings	estimated false positive findings*	FDR
#1	multiple sclerosis	30%	40 mm	13,947	177	0.0126
#2	multiple sclerosis	30%	40 mm	2,799	0	<0.0001
#3	Huntington disease	30%	40 mm	85,243	3,571	0.0419
#4	Huntington disease	30%	40 mm	64,272	0	<0.0001
#5	amyotrophic lateral sclerosis	15%†	40 mm	12,222	2,548	0.2085
#6	epilepsy post ATL	30%	40 mm	15,959	0	<0.0001
	normal control	30%	40 mm	74	0	N/A

* estimated by the number of tracks with increased anisotropic diffusion

†30% yields no findings

Supplementary Materials

Patient's medical history during the scan interval

MS patients

Patient #1 was a 44-year-old female with acute onset of left ocular pain and pain with eye movements. She experienced gradual decline in her visual acuity, and initial visual examination showed normal acuity in right eye and decreased acuity in left eye (20/70), which worsen to 20/400 in one week. She had a dense superior visual field defect in both superior quadrants that continued to worsen over few days with gradual loss of the inferior visual fields. She was treated with IV steroids, and after the treatment, the ocular pain, pain with eye movement, and the visual field were improved. After 6 months of her initial presentation, her visual acuity returned to 20/20 both eyes and the visual fields were normal

Patient #2 was a 23-year-old female with blurring of vision of the right eye, associated with ocular pain and pain with extra ocular movements. Initial evaluation by ophthalmology noted visual acuity of 20/40 with enlargement of the blind spot on the Humphrey visual field. Within a week her symptoms progressed to a visual acuity of 20/125, decrease in the color perception. and a superior altitudinal visual field defect. She was treated with intravenous methylprednisolone according to the optic neuritis treatment trial. Her symptoms recovered within 10 days to visual acuity of 20/25 and normal color saturation.

HD patients

Patient #3 was a 60-year-old male. The age of onset was 56, and the CAG repeats were 42. During the scan interval, the UHDRS motor total was increased from 45 to 49, with most prominent symptoms of body bradykinesia on both sides.

Patient #4 was a 55-year-old female. The age of onset was 48, and the CAG repeats were 43. During the scan interval, the UHDRS motor total was increased from 53 to 64, with symptoms of dystonic contractures of the left upper extremity, dragging right foot with ambulation, and dystonia in the legs more obvious with gait (mostly on the right side), moderate bradykinesia with the finger taps (mostly on the left side).

ALS patient

Patient #5 was a 48-year-old male ALS patient (laboratory supported probable ALS diagnosis) with upper extremity limb onset and predominant lower motor neuron involvement. His symptoms started about 30 months before the baseline scan with widespread fasciculations and left-hand weakness. There were subtle upper motor neuron signs in cervical segments. He developed lower extremity weakness 2 years after onset but never developed lower extremity upper motor neuron signs at the time of death that occurred 5 years after onset of symptoms. He had no family history of neurological disease. The patient's ALSFRS-R score decreased from 45 to 32 during the MRI scan interval (1 year apart).

Epilepsy patient

Patient #6 was a 51-year-old male with medically intractable epilepsy since the age of 17. His seizure frequency was weekly, and intracranial monitoring demonstrated that his seizure onset zone included the right mesial and neocortical temporal lobe. He underwent a standard right anterior temporal lobectomy. MRI scans were obtained before the surgery and one year after the surgery.